CIRA(EXT) 003

January 1996

Heat loss mechanisms in a measurement of specific heat capacity of graphite

D R Shipley and S Duane
Centre for Ionising Radiation and Acoustics
National Physical Laboratory
Teddington
Middlesex
United Kingdom
TW11 0LW

ABSTRACT

Absorbed dose to graphite in electron beams with nominal energies in the range 3–20 MeV is determined by measuring the temperature rise in the core of a primary standard graphite calorimeter. This temperature rise is related to absorbed dose by a separate measurement of the specific heat capacity of the graphite core. There is, however, a small but significant amount of heat lost from the sample in the determination of specific heat capacity and corrections for these losses are required. This report discusses the sources of heat loss in the measurements and, where possible, provides estimates for the magnitude of these losses. For those mechanisms which are significant, a more realistic model of the measurement system is analysed and corrections for the losses are provided.

Radiation from the sample to the surrounding environment was found to be the major source of heat loss in the measurement of specific heat capacity. The rate of heat loss by this process was at least one hundred times greater than the rate by any other process. A more realistic model of the measurement system (in which radiation was the only form of heat loss) indicated that, with a linear fit applied to the post-heating sample data, the extrapolated temperature rise requires a correction of 1.0003 ± 0.0001 (95% C.L.) to obtain the expected temperature rise of the sample. A correction of 0.9999 ± 0.0001 (95% C.L.) is required when a quadratic fit is used. The model and actual measurement system were found to agree to within a factor of two.

CIRA(EXT) 003

ISSN 1361-4053

National Physical Laboratory
Teddington, Middlesex, United Kingdom, TW11 0LW

Approved on behalf of Managing Director, NPL,
by Mr A J Marks, Director, Centre for Ionising Radiation and Acoustics

CONTENTS

Page

1 INTRODUCTION 1

2 HEAT TRANSFER MECHANISMS 1

2.1 NATURAL CONVECTION 1

CONDUCTION . 2

RADIATION . 3

3 EXPERIMENTAL PARAMETERS . 4

4 CONVECTION LOSSES IN THE MEASUREMENTS . 4

5 CONDUCTION AND RADIATION LOSSES IN THE MEASUREMENTS 5

5.1 CONDUCTION LOSSES BETWEEN SAMPLE AND SURROUNDING AIR 5

CONDUCTION LOSSES THROUGH CONNECTING THERMISTOR LEADS 6

5.2.1 Steady state temperature distribution 6
5.2.2 Time-dependent temperature distribution . 8
5.2.3 Coiling effects 10

5.3 RADIATION LOSSES TO SURROUNDING ENVIRONMENT 12

6 SUMMARY OF HEAT LOSSES 13

7 A MORE REALISTIC MODEL OF THE MEASUREMENT SYSTEM . 14

7.1 VARIATION OF SAMPLE AND JACKET TEMPERATURE WITH TIME 14

EXTRAPOLATION OF DATA 18

8 CONCLUSIONS 19

9 ACKNOWLEDGEMENTS 20

10 REFERENCES 20

ILLUSTRATIONS

Figure 1 Steady state temperature distributions with and without radiation losses in the thermistor leads. 8

Figure 2 Temperature distribution in the thermistor leads at different times. . 9

Figure 3 Cross section of thermistor wire in contact with sample.

Figure 4 Model of the sample/jacket measurement system used to determine the variation of sample and jacket temperature with time. 14

Figure 5 Variation of sample and jacket temperature with time: (a) during the heating period, and (b) after the heating period. 17

Figure 6 Linear least-squares fit to post-heating sample temperature data and corresponding residuals for the sample/jacket model. 18

Figure 7 Quadratic least-squares fit to post-heating sample temperature data and corresponding residuals for the sample/jacket model. 19

Figure A1.1 Model of the sample/mylar bag measurement system used to determine the variation of sample and bag temperature with time. 23

Figure A1.2 Variation of sample and mylar bag temperature with time: (a) during the heating period, and (b) after the heating period. 24

Figure A1.3 Linear least-squares fit to post-heating sample temperature data and corresponding residuals for the sample/mylar bag model. 25

Figure A1.4 Quadratic least-squares fit to post-heating sample temperature data and corresponding residuals for the sample/mylar bag model. 26

Figure A1.5 Model of the measurement system without any form of enclosure around the sample (except the belljar). 27

Figure A1.6 Variation of sample temperature with time: (a) during the heating period, and (b) after the heating period. 28

Figure A1.7 Linear least-squares fit to post-heating sample temperature data and corresponding residuals for the sample without enclosure model. 29

Figure A1.8 Quadratic least-squares fit to post-heating sample temperature data and corresponding residuals for the sample without enclosure model. 29

TABLES

Table 1 Typical values for various key quantities in experimental measurements with the sample/jacket system. 4

APPENDICES

Appendix 1 Other measurement systems 22

A1.1 Sample enclosed in an aluminised mylar bag 22

A1.2 Sample without an enclosure 26

1 INTRODUCTION

The National Physical Laboratory (NPL) is about to launch a new absorbed dose to water calibration service for electron beam radiotherapy. The service will be based on a primary standard graphite calorimeter which will measure absorbed dose to graphite in electron beams with nominal energies in the range 3–20 MeV. Absorbed dose to graphite is determined by measuring the temperature rise in the graphite core of the calorimeter as it is being irradiated. This temperature rise is related to absorbed dose by a separate measurement of the specific heat capacity of the graphite core. A factor is then applied to convert the calorimetric measurement of absorbed dose to graphite to absorbed dose to water.

The largest non-random uncertainty in the measurement of absorbed dose to graphite with the calorimeter is that associated with the specific heat capacity of the graphite core (approximately 0.7% (at 95% C.L.) compared with a total uncertainty of 1% (95% C.L.)). An attempt has therefore been made to determine this value more accurately and is described in detail by Williams et al.[1]. The specific heat capacity, c_s, of a given sample is found by dissipating a known amount of electrical energy E in a sample of known mass m_s and measuring the consequent temperature rise ΔT. The specific heat capacity, c_s, is then obtained using the following expression:

$$c_s = \frac{E}{m_s \Delta T} \tag{1}$$

In an ideal measurement system, all the energy applied to the sample contributes to the temperature rise. However, in practice, there is a small amount of heat lost from the system by various different processes. An estimate of these losses is therefore required to correctly determine the specific heat capacity of the sample. The purpose of this document is to discuss the mechanisms of heat loss that are occuring in the measurements of specific heat capacity and, if possible, provide an estimate of the magnitude of these losses. For those losses that are significant, a more realistic model of the measurement system is analysed and corrections for the losses are provided. This report is meant to be read in conjunction with the report by Williams et al.[1] in which details of the experimental apparatus design and construction are given. This document will concentrate on the analysis of heat losses in the sample/jacket measurement system presently used in the experimental setup. Two other measurement systems, also considered during the course of the work, are analysed in Appendix 1.

2 HEAT TRANSFER MECHANISMS

There are three distinct mechanisms by which heat is transferred from one body to another: convection, conduction and radiation. A brief overview of each process will be given in this section before analysing these mechanisms in the measurement of specific heat capacity.

2.1 NATURAL CONVECTION

Temperature gradients in a fluid cause variations in density from one point to another. Under gravity, these density variations setup pressure gradients which can drive fluid flow. This circulation leads to convective heat transfer, as warmer fluid in one region is displaced by cooler fluid from another. This is the dominant mode of heat transfer across air gaps under normal atmospheric pressure conditions. Bosworth[2] has reported the results of an experimental investigation of natural convection in air between horizontal and vertical parallel plates at different temperatures. These results were expressed in terms of a dimensionless Rayleigh number R in the form:

$$R = a\,d^3\,\Delta T \tag{2}$$

where ΔT is the temperature difference across the parallel plates (in K), d is the distance between them (in cm), and a is the convection modulus of air (in $\mathrm{cm^{-3}\,K^{-1}}$). When the Rayleigh number satisfies the inequality:

$$R < 1620 \tag{3}$$

no natural convection occurs. For air at 27°C and at atmospheric pressure, a has a value of $100\,\mathrm{cm^{-3}\,K^{-1}}$. Since a is proportional to the square of the density[2], the inequality in (3) may be rewritten in the form:

$$\left(\frac{P}{760}\right)^2 < \frac{16.2}{d^3\,\Delta T} \tag{4}$$

where P is the air pressure in millimetres of Hg. These conditions represent a very crude approximation to the system used to measure specific heat capacity and so the inequality in (4) will be used to deduce whether losses by natural convection are significant.

2.2 CONDUCTION

Conduction is the diffusion of heat along temperature gradients in a body as a result of intermolecular collisions. The rate at which heat flows along this temperature gradient ($dE/dt|_c$) is governed by the heat equation which can be written in the form:

$$\left.\frac{dE}{dt}\right|_c = kA\,\hat{\mathbf{n}}\cdot\nabla T \tag{5}$$

where k is the thermal conductivity of the medium, $\hat{\mathbf{n}}$ is a unit vector normal to the cross-sectional area A, and ∇T is the gradient of the temperature (in the direction of heat flow). In one dimension, this equation simplifies to the form:

$$\left.\frac{dE}{dt}\right|_c = -kA\,\frac{dT}{dx} \tag{6}$$

where dT/dx is the temperature gradient in the x direction. For conduction between two plane-parallel isothermal surfaces at temperatures T and T_0 ($T > T_0$) with a constant temperature gradient, the heat flow equation can be expressed as:

$$\left.\frac{dE}{dt}\right|_c = -h_c A(T - T_0) \tag{7}$$

where h_c is the conduction heat transfer coefficient which is proportional to the thermal conductivity k. For two isothermal parallel plates:

$$h_c = \frac{k}{d} \tag{8}$$

where d is the separation of the two plates. This expression will be used to estimate the heat flow along supporting strings and connecting wires in the measurement system. For heat flowing radially between concentric cylindrical surfaces[3]:

$$h_c = \frac{k}{r\,\ln(1 + d/r)} \tag{9}$$

where r is the inner cylinder radius and d is the separation of the cylindrical surfaces. The above equations will be used to calculate the conductive heat losses through air in the absence of natural convection between the surfaces—that is, provided the inequality in (4) holds.

2.3 RADIATION

Heat transfer by radiation involves the transport of electromagnetic energy from one body to another. The laws of thermal radiation take their simplest form for a *blackbody*. A blackbody absorbs all the radiation in the thermal spectrum falling upon its surface, reflecting and transmitting none. It is also a perfect radiator emitting energy at a rate depending solely on its surface temperature. For a blackbody at an absolute temperature T K, the rate at which energy is emitted as radiation (of all wavelengths), $dE/dt|_{r,bb}$ is given by the Stefan-Boltzmann law:

$$\left.\frac{dE}{dt}\right|_{r,bb} = A\sigma T^4 \tag{10}$$

where A is the surface area of the blackbody and σ is the Stefan-Boltzmann constant, which has the value 5.67×10^{-12} W cm^{-2} K^{-4}.

In general, however, the radiation falling on a material surface will be partly transmitted and reflected, and only partly absorbed. For this surface, the total radiation emitted at an absolute temperature T can be expressed in terms of the blackbody radiation at the same temperature and ε, the total emissivity of the surface:

$$\left.\frac{dE}{dt}\right|_{r} = \varepsilon A\sigma T^4$$

The total emissivity, ε, is defined as the ratio of the energy emitted by the surface to that which would be emitted by a blackbody at the same temperature. Highly polished metallic surfaces tend to have the smallest emissivities at room temperature and should be used wherever possible if radiative heat transfer is to be reduced. The emissivity of a surface also depends slightly on the surface temperature: however, for the small temperature ranges considered in this work, the emissivity is practically constant.

In a similar way, the fraction of incident radiation energy absorbed by the material surface is referred to as the absorptivity, α, of the material. The total absorptivity of a body is closely related to its total emissivity, and, at thermal equilibrium, they are the same according to a generalization known as Kirchoff's law.

The analysis of radiation losses in this work will consider the net rate of radiative heat transfer between a suspended body and its enclosure. A closed cavity or enclosure with walls at an absolute temperature T_0 is filled with radiation having a spectrum characterised by T_0 alone, and independent of the cavity wall material. A blackbody introduced into this cavity absorbs all incident radiation, and radiates at a rate appropriate to its own temperature T. At thermal equilibrium, T is equal to T_0 and the rates of emission and absorption are equal.

Since the sample and enclosure are not in fact 'black' and the temperature of these bodies are not equal, the final expression for the net rate of heat flow between the two bodies will be very complex since it must account for the many partial absorptions and reflections of the radiation at each surface and also the different geometries. One can, however, express the net rate of heat flow as follows:

$$\left.\frac{dE}{dt}\right|_{r} = A\sigma F(T^4 - T_0^4) \tag{12}$$

where F is a function of the emissivities of the two surfaces and their geometries, T is the absolute surface temperature of the suspended object and T_0 is the temperature of the enclosure. An approximation to the factor F for an object suspended in an enclosure is given by

Table 1 Typical values for various key quantities in experimental measurements with the sample/jacket system.

Quantity		Value
Radius of sample	r_s	1.55 cm
Height of sample		3.4 cm
Inner radius of jacket enclosure		4 cm
Inner height of jacket enclosure		9 cm
Environment temperature	T_0	297.65 K (24.5°C)
Environment pressure	P	$< 10^{-6}$ mm Hg
Heating thermistor temperature		322.65 K ($T_0 + 25$°C)
Power input	$\dot{E}_{in}$	39.0 mW
Sample heating time	t_{heat}	15.0 s
Sample temperature rise	$\Delta T_{s,m}$	16.39 mK
Sample specific heat capacity	c_s	715.75 J kg^{-1} K^{-1}
Pre-heating temperature drift		0.101 mK min^{-1}
Post-heating temperature drift		0.211 mK min^{-1}

McAdams[4]. This is used in the present work and takes the form:

$$F = \frac{1}{(1/\varepsilon) + (A/A_0)[(1/\varepsilon_0) - 1]} \tag{13}$$

where ε is the emissivity of the object and ε_0 is the emissivity of the enclosure; A and A_0 are the total surface areas of the object and enclosure respectively. If $A \ll A_0$, then F is approximately equal to ε, and the enclosure behaves like a blackbody.

3 EXPERIMENTAL PARAMETERS

Typical values for various key quantities in the experimental measurements are given in Table 1. These values will be used in the analysis of the sample/jacket system to estimate the magnitude of heat lost by the different processes mentioned above. The temperature rise of the sample along with the pre- and post-heating temperature drifts for one particular set of measurements are also given for completeness. The value quoted for the specific heat capacity of graphite c_s was obtained using the expression, $c_s = 644.9 + 2.94T_0(°C)$, quoted by Williams et al.[1]

4 CONVECTION LOSSES IN THE MEASUREMENTS

Consider the inequality given in equation (4). For the measurements being considered[1], d can be taken to be the separation between the surface of the sample and the graphite jacket. Natural convection will not occur at atmospheric pressure ($P = 760$ mm Hg) provided that ΔT is less than 1.1°C. Temperature differences of this magnitude do occur between the jacket and parts of sample in the measurements, particularly during the heating period, making convection losses possible at this pressure. The enclosure is evacuated in the measurements. At a pressure of 10^{-3} mm Hg (below which the fluid model of air breaks down since the molecular mean free path of air exceeds the separation of the surfaces d) the inequality in (4) is satisfied by a factor of 10^{11}. Indeed, the actual pressure used is less than 10^{-6} mm Hg and so natural convection is physically impossible.

5 CONDUCTION AND RADIATION LOSSES IN THE MEASUREMENTS

These are the dominant modes of heat loss from the sample to the environment in the measurement of specific heat capacity. There are in fact various different routes by which heat is transferred to the environment. Each will be examined in turn in this section to determine which contribute most significantly to the observed heat losses.

5.1 CONDUCTION LOSSES BETWEEN SAMPLE AND SURROUNDING AIR

An initial estimate of the conductive heat losses from the sample to the surrounding air may be obtained using the one dimensional expression (from equations (7) and (8)):

$$\left.\frac{dE}{dt}\right|_{c} = -\frac{k_{air}}{d} A(T_s - T_j) \tag{14}$$

Here, one assumes that the sample and the graphite jacket form two plane parallel isothermal surfaces with a constant temperature gradient between them. Taking the average surface temperature of the sample to be 16 mK above the jacket temperature (as observed in the measurements), that is, $T_s - T_j = 0.016$, and the thermal conductivity of air, k_{air}, to be 2.41×10^{-4} W cm^{-1} K^{-1} (at 1 atmosphere), then the average rate of heat loss by conduction to the surroundings per unit surface area of the sample will be approximately 2×10^{-6} W cm^{-2} (or 8×10^{-5} W from the whole sample surface). This value could increase up to 2×10^{-3} W cm^{-2} on parts of the sample near the heating thermistor during the heating period where sample-jacket temperature differences may be as high as 25 K.

A slightly better estimate to the one dimensional case for conductive heat losses may be obtained by assuming the sample and jacket take the form of two isothermal concentric cylinders with a constant temperature gradient. The conductive heat flow equation for this geometry is given by (from equations (7) and (9)):

$$\left.\frac{dE}{dt}\right|_{c} = -\frac{k_{air}}{r \ln(1 + d/r)} A(T_s - T_j) \tag{15}$$

where r is taken to be the radius of the sample. In this case, the average rate of heat loss by conduction from the sample is 3×10^{-6} W cm^{-2} (or 1×10^{-4} W from the whole surface) with peak losses of up to 4×10^{-3} W cm^{-2}.

These calculations are valid for a conducting medium of air at 1 atmosphere (760 mm Hg) and 0°C whereas in the experimental measurements an air pressure of $< 10^{-6}$ mm Hg is used. The thermal conductivity of air is proportional to the following factors[3] :

$$k_{air} \propto \rho \bar{v} \lambda c_v$$

where ρ is the density of air (proportional to the pressure), $\bar{v}$ is the mean molecular velocity (independent of pressure), λ is the mean free path between molecular collisions (inversely proportional to the pressure), and c_v is the heat capacity at constant volume. The thermal conductivity, k_{air}, is therefore independent of the pressure, as long as the mean free path is small compared to the separation of the two surfaces (that is, the air behaves as a fluid). However, as the pressure is reduced, and the mean free path becomes comparable to the separation of the surfaces, the intermolecular collisions become less frequent and the above equation no longer holds. Instead (at pressures below approximately 10^{-3} mm Hg), Laughlin and Genna[3] have shown that the heat transfer coefficient, h_c, for air (which is proportional to the thermal conductivity) becomes:

$$h_c = 9.2 \times 10^{-3} P$$

where P is the air pressure in mm Hg. As one would expect, the heat transfer coefficient for free molecular motion is independent of the separation between the two surfaces. This equation is valid for plane parallel surfaces and is also an adequate approximation of h_c for concentric surfaces. With an air pressure of 10^{-6} mm Hg, h_c has a value of 9.2×10^{-9} W cm^{-2} K^{-1}, and the average rate of heat loss by conduction from the sample to the surrounding air will be approximately 2×10^{-10} W cm^{-2} (7×10^{-9} W from whole surface) and up to 2×10^{-7} W cm^{-2} near the heating thermistor during the heating period.

5.2 CONDUCTION LOSSES THROUGH CONNECTING THERMISTOR LEADS

These losses are estimated for a number of different temperature distributions in the sensing and heating thermistor leads and initially assume the heating wires are *not* coiled around the sample. The effect of coiling these wires around the sample, as in the experimental setup, to reduce heat losses is investigated later in Section 5.2.3.

5.2.1 Steady state temperature distribution

The simplest model for conduction through the connecting thermistor leads assumes that the ends of each wire form two plane parallel isothermal surfaces with a steady state temperature distribution existing between them. If there are no other mechanisms of heat transfer in the system, then the steady state temperature distribution, $T_w(x)$, along the wire satisfies Laplace's equation in one dimension:

$$\frac{d^2}{dx^2}(T_w(x) - T_j) = 0 \tag{18}$$

where x is the distance along the wire. By solving this equation and applying boundary conditions, the steady-state temperature distribution in the wire for this model is found to be:

$$T_w(x) = T_s - \left(\frac{T_s - T_j}{L}\right) x$$

where T_s and T_j are the temperatures at the sample and jacket end of the wire (assumed fixed), and L is the total length of the wire. Taking the length of each sensing thermistor wire to be 5 cm and the temperature difference between the ends to be 16 mK (the typical temperature difference observed between sample and jacket), the rate of heat loss by conduction through each sensing thermistor wire is 5.5×10^{-7} W (using equation (6) with equation (19)). In the case of the *uncoiled* heating thermistor wires (each of length 32 cm), where the temperature difference between the ends reaches approximately 25 K during the heating period, the rate of heat loss through each wire could be as high as 1.4×10^{-4} W. After the heating period, however, the temperature of the heating thermistor rapidly returns towards the average sample temperature. The heat lost by conduction through each heating thermistor wire during the period after heating is therefore expected to be the same as for the sensing thermistor wires.

A better estimate of the heat losses by conduction through the connecting thermistor leads may be obtained by extending the above model to include radiation losses from the wires. (Other heat loss mechanisms such as natural convection from the wires and conduction between the wires and the surrounding environment will be negligible according to the analyses in Sections 4 and 5.1). Using equation (6) (for conduction losses in one dimension), equation (12) with (13) (for radiation losses) and the conservation of energy, the steady state temperature distribution, $T_w(x)$, at a distance x along the wire for this more refined model can be shown to satisfy the following differential equation:

$$\frac{d^2}{dx^2}(T_w(x) - T_j) = \alpha^2 (T_w(x) - T_j)$$

where T_j is the temperature at the jacket end of the wire. The parameter α is defined as follows:

$$\alpha^2 = \frac{8\sigma\varepsilon_w T_j^3}{r_w k_w} \tag{21}$$

where σ is the Stefan-Boltzmann constant, ε_w is the emissivity of the thermistor wire[(1)] (= 0.07[5]), r_w is the measured radius (3.78×10^{-3} cm) and k_w is the thermal conductivity of the wire ($\equiv k_{Cu} = 3.85\ \mathrm{W\,cm^{-1}\,K^{-1}}$). Solving this differential equation for $T_w(x)$ and applying boundary conditions gives the following expression for the steady state temperature distribution in the wire:

$$T_w(x) = T_j + \frac{T_s - T_j}{\sinh(\alpha L)} \sinh(\alpha(L - x)) \tag{22}$$

where T_s is the temperature at the sample end of the wire. A plot of this temperature distribution is shown in Figure 1: the steady-state distribution ignoring radiation losses is also shown for comparison. As can be seen from these distributions, when radiation losses are taken into account, the rate at which heat is conducted along the wire varies along its length and is greatest near the point of contact with the sample. Evaluating the rate of heat flow at this point provides an estimate of the rate of heat loss by conduction from the sample along the connecting thermistor leads. Using equation (6) with the temperature distribution in equation (22) and evaluating at $x = 0$, the rate of heat loss from the sample along each sensing thermistor wire is 5.8×10^{-7} W and along each uncoiled heating thermistor wire (during the heating period) is 3.3×10^{-4} W.

The rate at which heat is conducted through the other end of each thermistor wire (that is, at $x = L$) is also found in a similar way. Here, the conductive heat flow rates in the sensing and heating thermistor wires are 5.4×10^{-7} W and 5.8×10^{-5} W respectively. From the original analysis, the difference in the conduction rates at the ends of each wire corresponds to the rate at which heat is lost by radiation from the wire (by conservation of energy). Thus, in the sensing thermistor wires, approximately 7% of the conducted energy is lost by radiation whereas, in the uncoiled heating thermistor wires (during the heating period), up to 83% of the conducted energy is radiated. These radiative heat loss values depend significantly on the value of ε_w used for the thermistor leads. For example, with ε_w equal to 0.20, the proportion of conducted heat lost by radiation from the sensing and uncoiled heating thermistor leads increases to 18% and 97% respectively.

[(1)]For the purpose of this work, the emissivity of each thermistor lead was assumed to be the same as the emissivity of copper. Ideally, the emissivity of the enamel insulation coating the leads should be used instead but this data was not available.

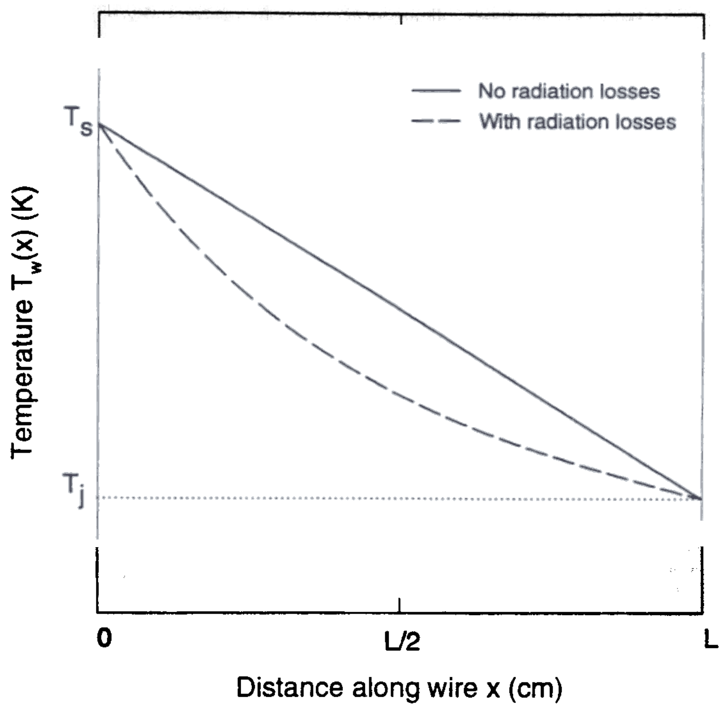

Figure 1 Steady state temperature distributions with and without radiation losses in the thermistor leads.

The question that remains is how relevant is the assumption that steady state conditions exist in the connecting thermistor leads. As a rough indication of how long it takes to establish equilibrium conditions in the wires, one can compare the total heat content in the wire, $E_{w,tot}$ with the rate at which energy is conducted into the wire from the sample, $dE/dt|_{c,w}$, both evaluated in the steady state. Now:

$$E_{w,tot} = \pi r_w^2 \rho_w c_w \int_0^L (T_w(x) - T_j)\, dx$$

where r_w is the radius, ρ_w is the density (8.96 g cm^{-3}) and c_w is the specific heat capacity (385 J kg^{-1} K^{-1}) of the wire. For the steady state distribution given in equation (22), $E_{w,tot}$ is given by:

$$E_{w,tot} = \pi r_w^2 \rho_w c_w (T_s - T_j) \cdot \frac{(\cosh(\alpha L) - 1)}{\alpha \sinh(\alpha L)}$$

with α defined as before (equation (21)). Dividing $E_{w,tot}$ by $dE/dt|_{c,w}$ gives:

$$\tau_{ss} \equiv \frac{E_{w,tot}}{dE/dt|_{c,w}}$$

a quantity having the dimension of time. Based on this equation, the time τ_{ss} for the heating thermistor wires is 128 seconds. This is much greater than the sample heating time (typically 15 s) and so it is clear that one must consider the time dependent temperature distribution in the wires.

5.2.2 Time-dependent temperature distribution

As in the previous section, we again assume that the ends of each wire form two plane parallel isothermal surfaces at temperatures T_s and T_j and that conduction and radiation are the only

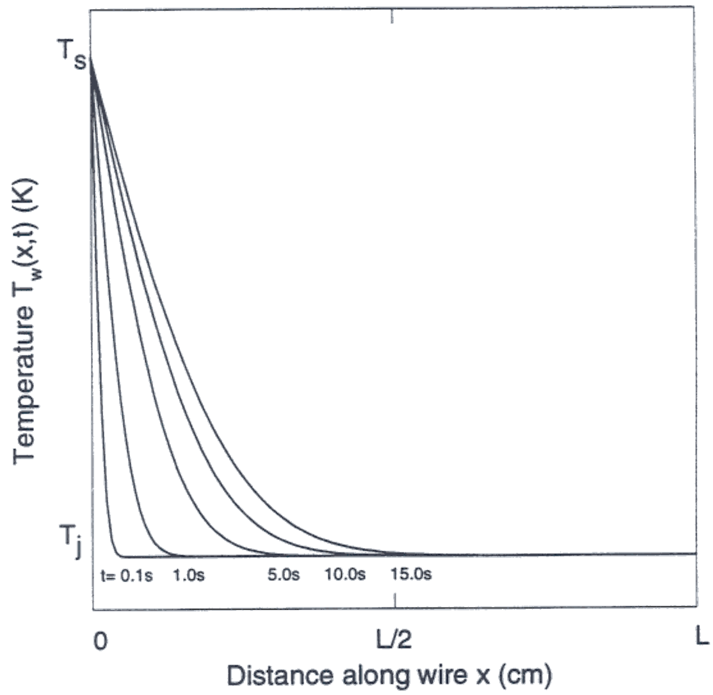

Figure 2 Temperature distribution in the thermistor leads at different times.

heat transfer mechanisms in the wire. Then, by conservation of energy, the time-dependent temperature distribution, $T_w(x,t)$, in the wire satisfies the following differential equation:

$$\frac{d^2}{dx^2}(T_w(x,t) - T_j) - \alpha^2 (T_w(x,t) - T_j) = \beta \frac{d}{dt}(T_w(x,t) - T_j)$$

where α has the same definition as before (equation (21)) and β is defined as:

$$\beta = \frac{\rho_w c_w}{k_w}$$

where ρ_w and c_w are the density and specific heat capacity of the wire. Solving this equation for $T_w(x,t)$ and applying boundary conditions at the ends of the wire (assuming an initial instantaneous temperature rise at the sample end), the time dependent temperature distribution in the wire has the form:

$$T_w(x,t) = T_j + (T_s - T_j)\left[\frac{\sinh(\alpha(L-x))}{\sinh(\alpha L)} - \frac{2}{L}\sum_{n=1}^{\infty}\left(\frac{n\pi/L}{\alpha^2 + (n\pi/L)^2}\right)\exp(-\omega_n^2 t)\sin\frac{n\pi x}{L}\right]$$

where ω_n is defined as follows:

$$\omega_n^2 = \frac{\alpha^2 + (n\pi/L)^2}{\beta}, \quad n = 1, 2, \ldots$$

The temperature distribution, $T_w(x,t)$, has been expressed in terms of the steady state distribution derived in the previous section (equation (22)) with a time-dependent term that vanishes as $t \rightarrow \infty$. A plot of this temperature distribution with distance along the wire at different times is shown in Figure 2. From these plots, one can deduce that the rate of heat flow by conduction along the wire near the point of contact with the sample (that is, at $x = 0$) is initially infinite (as expected for an instantaneous temperature rise) and then decreases rapidly towards a constant steady state value (discussed in the previous section). Evaluating the conductive heat flow rate at this point for a given time provides an estimate of the rate of heat loss by conduction from the sample along the connecting thermistor wires in the experimental measurements. At the end of the heating period ($t = t_{\mathrm{heat}}$), the conductive heat losses through each sensing and heating thermistor wire are estimated to be 5.8×10^{-7} W and 6.5×10^{-4} W respectively. The conductive heat loss through the opposite end of each sensing thermistor wire (at $x = L$) is 5.4×10^{-7} W but is negligible in the uncoiled heating thermistor wires. The total energy, $E_{\mathrm{c,tot}}$, conducted into each wire during this period is found using the following expression:

$$E_{\mathrm{c,tot}} = -\pi r_{\mathrm{w}}^2 k_{\mathrm{w}} \int_0^{t_{\mathrm{heat}}} \frac{d}{dx}(T_{\mathrm{w}}(0,t) - T_{\mathrm{j}})\, dt \tag{30}$$

where $T_{\mathrm{w}}(0,t)$ is the time dependent temperature distribution in the wire near the point of contact with the sample. Expanding this expression gives:

$$\begin{aligned} E_{\mathrm{c,tot}} &= -\pi r_{\mathrm{w}}^2 k_{\mathrm{w}} (T_{\mathrm{s}} - T_{\mathrm{j}}) \Bigg[\left(\frac{\alpha \cosh(\alpha L)}{\sinh(\alpha L)} \right) t_{\mathrm{heat}} + \\ & \frac{2}{L} \sum_{n=1}^{\infty} \left[\frac{(n\pi/L)^2}{\alpha^2 + (n\pi/L)^2} \right] \frac{1}{\omega_{\mathrm{n}}^2} \left(\exp(-\omega_{\mathrm{n}}^2 t_{\mathrm{heat}}) - 1 \right) \Bigg] \end{aligned}$$

and evaluating for each sensing and heating thermistor wire gives values for $E_{\mathrm{c,tot}}$ of 1.27×10^{-5} J and 1.84×10^{-2} J respectively. These values assume that the wires initially have zero energy content and that the heating thermistor leads are uncoiled. The total energy deposited in the sample during the heating period is 0.585 J ($\dot{E}_{\mathrm{in}} \times t_{\mathrm{heat}}$) and thus up to 3% of this energy is lost by conduction through each heating thermistor wire (uncoiled).

The total energy lost by radiation, $E_{\mathrm{r,tot}}$, from the wires during the heating period may be estimated using the following expression (from equations (12) and (13)):

$$E_{\mathrm{r,tot}} = 2\pi r_{\mathrm{w}} \sigma \varepsilon_{\mathrm{w}} \int_0^{t_{\mathrm{heat}}} \left[\int_0^L ([T_{\mathrm{w}}(x,t)]^4 - T_{\mathrm{j}}^4)\, dx \right] dt \tag{32}$$

where $T_{\mathrm{w}}(x,t)$ is the temperature distribution in the wire as a function of distance and time (equation (28)). For small temperature differences (that is, $T_{\mathrm{w}}(x,t) \approx T_{\mathrm{j}}$), $E_{\mathrm{rad,tot}}$ has the form:

$$\begin{aligned} E_{\mathrm{r,tot}} &= 8\pi r_{\mathrm{w}} \sigma \varepsilon_{\mathrm{w}} T_{\mathrm{j}}^3 (T_{\mathrm{s}} - T_{\mathrm{j}}) \Bigg[\left(\frac{\cosh(\alpha L) - 1}{\alpha \sinh(\alpha L)} \right) t_{\mathrm{heat}} - \\ & \frac{2}{L} \sum_{n=1}^{\infty} \left[\frac{1}{\alpha^2 + (n\pi/L)^2} \right] \frac{1}{\omega_{\mathrm{n}}^2} ((-1)^n - 1) \left(\exp(-\omega_{\mathrm{n}}^2 t_{\mathrm{heat}}) - 1 \right) \Bigg] \end{aligned} \tag{33}$$

where ω_{n}, α and β are defined as before. With this expression for $E_{\mathrm{r,tot}}$, the energy lost by radiation from the sensing and uncoiled heating thermistor leads during the heating period is 5.17×10^{-7} J and 1.13×10^{-3} J respectively. This is approximately 4% of the total energy conducted from the sample along the sensing thermistor wires and 6% of the energy conducted along the uncoiled heating thermistor wires (assuming ε_{w} is equal to 0.07).

5.2.3 Coiling effects

The discussion has so far neglected the fact that the heating thermistor leads are wrapped around the sample several times to reduce conductive and radiative heat losses from the wires (which would otherwise be significant according to our earlier discussions). The effect of coiling the wires around the sample on the magnitude of these heat losses is investigated in this section.

Consider the system shown in Figure 3 which shows a uniform length of wire in good thermal contact with a graphite sample. If we assume that:

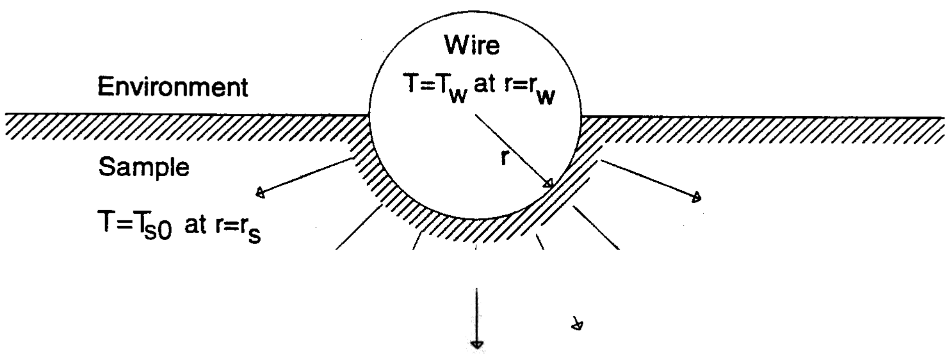

Figure 3 Cross section of thermistor wire in contact with sample.

(i) half the surface area of the wire is in contact with the sample,

(ii) a steady state temperature distribution exists within the wire,

(iii) the temperature along the length of wire in contact with the sample is approximately constant (that is, the wire is a very efficient conductor of heat), and,

(iv) conductive heat losses between the wire and the sample do not vary with angle about the wire axis,

then, the radial temperature distribution, $T_s(r)$, in the sample at a distance r from the centre of the wire satisfies Laplace's equation in cylindrical coordinates, that is:

$$\nabla^2 T_s(r) = 0$$

or:

$$\frac{1}{r}\frac{d}{dr}\left[r\frac{d}{dr}(T_s(r))\right] = 0 \tag{35}$$

Solving this equation and applying boundary conditions gives the following radial temperature distribution in the sample:

$$T_s(r) = T_{s0} + \frac{(T_W - T_{s0})}{\ln(r_W/r_s)}\ln\frac{|r|}{r_s}, \quad r_W < r < r_s$$

where T_{s0} is the temperature at the centre of the sample (taken to be at $r = r_s$, assumed fixed), T_W is the surface temperature of the wire, and r_s and r_W are the radii of the sample and wire respectively. The total conductive heat flow, $dE/dt|_{c,s}$, from the wire back into the sample for this temperature distribution can then be found using equation (5) evaluated at $r = r_W$ with the temperature gradient $\hat{\mathbf{n}} \cdot \nabla(T_s(r) - T_{s0})$ expressed in cylindrical coordinates. The heat flow, $dE/dt|_{c,s}$, then has the form:

$$\left.\frac{dE}{dt}\right|_{c,s} = \kappa(T_W - T_{s0})$$

with the constant of proportionality κ given by:

$$\kappa = -\frac{\pi L_c k_s}{\ln(r_W/r_s)}$$

where L_c is the length of wire in contact with the sample and k_s is the thermal conductvity of the sample.

In the experimental setup, L_c for each heating thermistor wire is 22 cm and r_w and r_s are 3.78×10^{-3} cm and 1.55 cm respectively. Taking k_s for graphite to be 0.05 W cm^{-1} K^{-1}, the rate at which energy is conducted from the wire back into the sample per K temperature difference (= κ) is 0.574 W K^{-1}. During the heating period, $(T_w - T_{s0})$ near the heating thermistor is typically 25 K which gives a value for $dE/dt|_{c,s}$ of 14.4 W. This value is several orders of magnitude larger than the rate at which heat is lost from the sample along the uncoiled heating thermistor leads during the heating period (~ 10^{-4} W). This is still true even if the area of contact between the wire and the sample is reduced to just 1% (equivalent to reducing r_w by a factor of 50 in the model). The value of $dE/dt|_{c,s}$ during the heating period in this case is 9.4 W. Of course, no more heat can flow back into the sample than can flow into the thermistor end of the wire. What actually happens is that the temperature falls rapidly along the length of wire in contact with the sample, and thus assumption (iii) is not valid and the model does not apply. Nevertheless, we conclude that only a small area of contact between the heating thermistor wire and the sample is sufficient to ensure that essentially all the heat that flows into the wire from the thermistor subsequently flows back into the sample, and is not lost.

5.3 RADIATION LOSSES TO SURROUNDING ENVIRONMENT

The net rate of heat loss by thermal radiation from the sample to the surrounding environment may be estimated using the following expression (from equation (12)):

$$\left.\frac{dE}{dt}\right|_r = A_s \sigma F_s (T_s^4 - T_j^4) \tag{39}$$

where the factor F_s, for the sample suspended in the graphite enclosure, is taken to be (from equation (13)):

$$F_s = \frac{1}{(1/\varepsilon_s) + (A_s/A_j)[(1/\varepsilon_j) - 1]} \tag{40}$$

In these equations, A_s is the total surface area of the sample (48.2 cm^2) and A_j is the inner surface area of the graphite jacket (326.7 cm^2). The terms ε_s and ε_j are the corresponding emissivities of the two surfaces which are taken to be 0.75 ($\equiv \varepsilon_{\text{graphite}}$) and 0.05 ($\equiv \varepsilon_{\text{Al}}$) respectively. The emissivity for aluminium is chosen in the latter case since the inner surface of the jacket is completely covered with a sheet of aluminised mylar in the experimental setup. The mylar sheet is assumed be in good thermal contact with the graphite jacket and to have negligible heat capacity. Taking the average surface temperature of the sample (T_s) to be 297.666 K and of the jacket (T_j) to be 297.65 K (from Table 1), the net rate of radiative heat loss from the sample is approximately 2.3×10^{-6} W cm^{-2} or 1.1×10^{-4} W from the whole surface. This value is within an order of magnitude of the observed heat loss in the experimental measurements (6.6×10^{-5} W derived from the data in Table 1).

On parts of the sample surface near the heating thermistor, the temperature difference between the sample and jacket may be as high as 25 K during the heating period (depending on the thermal conductivities of the thermistor glass, heat sink, etc) resulting in radiative heat losses of up to 4.1×10^{-3} W cm^{-2} from these areas. A significant proportion of the electrical input energy may therefore be lost by radiation during this period. This loss, however, should be accounted for in the extrapolation of the temperature data (Section 7.2) if, as assumed in this work, the surface temperature measured by the sensing thermistor closely matches the average surface temperature of the sample. If the measured temperature is less than the average surface temperature (which is possible since the sample temperature is measured at only one point on the surface), the extrapolated temperature rise of the sample will be underestimated thus giving a higher than normal value for it's specific heat capacity. One could find out whether this is in fact the case by determining the temperature distribution over the sample surface during the heating period. The analysis, however, is quite difficult and time-consuming and could not be done during the course of this work.

6 SUMMARY OF HEAT LOSSES

All the possible mechanisms of heat loss from the sample in the specific heat capacity measurements have now been analysed. These heat losses will be summarised in this section and their magnitudes compared to determine which are the most dominant mechanisms in the measurements. The heat lost from the sample in the experimental measurements is estimated to be 6.6×10^{-5} W (from the observed post-heating temperature drift in Table 1).

Losses by natural convection from the sample (and also from the connecting thermistor leads) have been shown to be significant at atmospheric pressure. However, by evacuating the system to less than 10^{-6} mm Hg, as in the experimental setup, these losses are completely negligible since convection cannot occur. This is similarly true for conduction losses (through the air) between the sample (and leads) and the surrounding environment. In this case, the average rate of heat loss from the sample surface at atmospheric pressure is estimated to be in the range $0.8\text{–}1 \times 10^{-4}$ W (with a peak loss of $2\text{–}4 \times 10^{-3}$ W cm^{-2} near the heating thermistor during the heating period) whereas, at pressures of $< 10^{-6}$ mm Hg, the average loss is only 7×10^{-9} W (2×10^{-7} W cm^{-2} near the heating thermistor).

Conduction losses from the sample along the connecting thermistor leads are much more significant. Initially, these losses were estimated for two different steady state temperature distributions in each wire but it was subsequently shown that steady state conditions could not exist in the wires during or soon after the heating period. The time dependent temperature distribution in the wires was therefore obtained. With this distribution, the conductive heat losses along the sensing and *uncoiled* heating thermistor wires at the end of the heating period (t_{heat} = 15 s) are estimated to be 5.8×10^{-7} W and 6.5×10^{-4} W respectively. The total energy conducted into each wire during this period is approximately 1.3×10^{-5} J and 1.8×10^{-2} J respectively: 4–6% of this energy is lost by radiation from the wires (assuming a small emissivity).

When the heating thermistor leads are uncoiled (as initially assumed in the calculations), the conductive heat losses along these wires during the heating period are very large (approximately 1100 times greater than the losses along the sensing thermistor wires) and are comparable with the observed heat losses in the measurements. However, by coiling the heating thermistor leads around the sample, as in the experimental setup, these losses are greatly reduced. In this case, virtually all of the heat lost by conduction into the heating thermistor leads is conducted almost immediately back into the sample: the remaining length of wire in contact with the sample is held at the sample temperature. The radiation losses from these leads are therefore small for most of their length (with similar losses to the sensing thermistor wires) except near the heating thermistor itself where losses during the heating period are thought to be slightly greater. To reduce these radiation losses to a minimum, the lengths of wire between the heating thermistor and the sample should be kept as small as possible.

Radiation from the sample to the surrounding environment is by far the greatest source of heat loss in the experimental measurements. The average rate of radiative heat loss from the sample surface is approximately 1.1×10^{-4} W with peak losses of up to 4.1×10^{-3} W cm^{-2} on parts of the sample near the heating thermistor during the heating period. This is approximately two orders of magnitude greater than the conductive losses from the sample along the

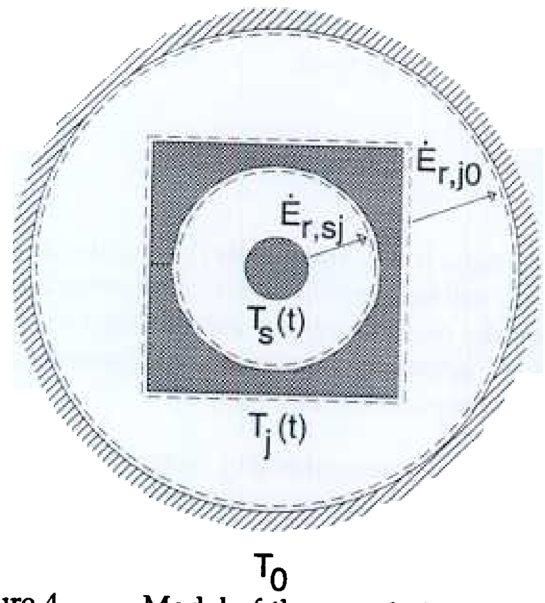

Figure 4 Model of the sample/jacket measurement system used to determine the variation of sample and jacket temperature with time. Radiation is the only form of heat transfer in the system.

connecting thermistor leads (although it would be comparable to the losses along the heating thermistor wires if they were uncoiled), and is within 40% of the observed heat loss in the measurements.

7 A MORE REALISTIC MODEL OF THE MEASUREMENT SYSTEM

The previous section has shown that radiation from the sample is the dominant form of heat loss in the experimental measurements (with other mechanisms shown to be negligible). A more realistic model of the sample/jacket system will now be analysed in which radiation is the only form of heat transfer between the individual components. The variation of the sample and jacket temperature with time during and after the heating period will first be derived and compared with measured temperature profiles. Extrapolation techniques similar to those used in the experimental measurements to eliminate the effect of heat losses from the system will then be applied to obtain the actual temperature rise of the sample. This temperature rise will be compared with the expected temperature rise of the sample (with no heat loss) and corrections derived where necessary.

Two other measurement systems were also considered during the course of the work to determine specific heat capacity. In one, the sample was enclosed in an aluminised mylar bag instead of a graphite jacket, and in the other, the sample had no form of enclosure except the belljar: these systems are analysed in Appendix 1.

7.1 VARIATION OF SAMPLE AND JACKET TEMPERATURE WITH TIME

The model adopted to determine the variation of sample and jacket temperature during and after the heating period is shown in Figure 4. It consists of a graphite sample, with an average surface temperature $T_s(t)$, enclosed in a graphite jacket, at temperature $T_j(t)$, which itself is enclosed in an evacuated belljar held at a fixed environment temperature T_0. The inner and outer surfaces of the graphite jacket and the inner surface of the belljar are completely covered in aluminised mylar which is assumed to be in good thermal contact with the graphite and have negligible heat capacity. (If the thermal contact between the aluminised mylar and jacket is poor, then this system would act in a similar way to the sample/bag system analysed in Appendix 1). The model also assumes that the sample has a high thermal conductivity (i.e. a negligible relaxation time) and that radiation is the only form of heat transfer. In identifying these model parameters with the measurement system, it is assumed that the temperature measured by the sensing thermistor represents the average surface temperature of the sample. This is not unreasonable since the heating and sensing thermistors are positioned 90° apart on the cylindrical surface of the sample. With these assumptions, one may write down the following four coupled differential equations which govern the rate of heat transfer in the system:

$$\begin{aligned}
\dot{E}_{r,sj} \equiv \left.\frac{dE}{dt}\right|_{r,sj} &= A_s \sigma F_s([T_s(t)]^4 - [T_j(t)]^4) \\
\dot{E}_{r,j0} \equiv \left.\frac{dE}{dt}\right|_{r,j0} &= A_{outj} \sigma F_j([T_j(t)]^4 - T_0{}^4) \\
\dot{E}_{r,sj} - \dot{E}_{r,j0} &= m_j c_j \frac{d}{dt}(T_j(t)) \\
\dot{E}_{in} - \dot{E}_{r,sj} &= m_s c_s \frac{d}{dt}(T_s(t))
\end{aligned}$$

with the factors F_s and F_j for the sample and jacket given by:

$$\begin{aligned}
F_s &= \frac{1}{(1/\varepsilon_s) + (A_s/A_{inj})[(1/\varepsilon_{inj}) - 1]} \\
F_j &= \frac{1}{(1/\varepsilon_{outj}) + (A_{outj}/A_0)[(1/\varepsilon_0) - 1]}
\end{aligned}$$

where:

$\dot{E}_{r,sj}$ is the net rate of heat transfer by radiation between the sample and jacket,

$\dot{E}_{r,j0}$ is the net rate of heat transfer between the jacket and belljar,

$\dot{E}_{i}$ is the rate at which the sample is heated, that is, the power input (assumed constant),

m_s, m_j are the masses of the sample and jacket,

c_s, c_j are the specific heat capacities of the sample and jacket,

A_s is the total surface area of the sample,

A_{inj}, A_{outj} are the total inner and outer surface areas of the graphite jacket,

A_0 is the total inner surface area of the belljar enclosure,

ε_s is the emissivity of the sample surface,

ε_{inj}, ε_{outj} are the emissivities of the inner and outer surfaces of the graphite jacket, and,

ε_0 is the emissivity of the inner surface of the belljar.

Combining these four equations and rearranging gives the following two first-order linear differential equations (for small temperature differences, that is, $T_s(t) \approx T_j(t) \approx T_0$):

$$\begin{aligned} \frac{d}{dt}(T_j(t)) + \alpha_1 T_j(t) + \alpha_2 T_s(t) &= \alpha_3 \\ \frac{d}{dt}(T_s(t)) + \beta_1 T_j(t) + \beta_2 T_s(t) &= \beta_3 \end{aligned}$$

which in matrix notation becomes:

$$\begin{pmatrix} \dot{T}_j(t) \\ \dot{T}_s(t) \end{pmatrix} + \begin{pmatrix} \alpha_1 & \alpha_2 \\ \beta_1 & \beta_2 \end{pmatrix} \begin{pmatrix} T_j(t) \\ T_s(t) \end{pmatrix} = \begin{pmatrix} \alpha_3 \\ \beta_3 \end{pmatrix}$$

where the parameters α_1–α_3 and β_1–β_3 are defined as follows:

$$\alpha_1 = \frac{4\sigma T_0^3 (F_s A_s + F_j A_{outj})}{m_j c_j}, \quad \alpha_2 = -\frac{4\sigma T_0^3 F_s A_s}{m_j c_j}, \quad \alpha_3 = \frac{4\sigma T_0^4 F_j A_{outj}}{m_j c_j}$$

$$\beta_1 = -\frac{4\sigma T_0^3 F_s A_s}{m_s c_s}, \quad \beta_2 = \frac{4\sigma T_0^3 F_s A_s}{m_s c_s}, \quad \beta_3 = \frac{\dot{E}_{in}}{m_s c_s} \tag{51}$$

The general solution of this inhomogeneous system for $T_j(t)$ and $T_s(t)$ has the form:

$$\begin{pmatrix} T_j(t) \\ T_s(t) \end{pmatrix} = \begin{pmatrix} T_{j,eqm} \\ T_{s,eqm} \end{pmatrix} + C_+ \exp(-\lambda_+ t)\, \mathbf{e}_+ + C_- \exp(-\lambda_- t)\, \mathbf{e}_- \tag{52}$$

where λ_+ and λ_- are the eigenvalues of the system, which are given by the following expression:

$$\lambda_\pm = \frac{1}{2}\left[(\alpha_1 + \beta_2) \pm \sqrt{(\alpha_1 + \beta_2)^2 - 4(\alpha_1\beta_2 - \alpha_2\beta_1)}\right], \tag{53}$$

$\mathbf{e}_+$ and $\mathbf{e}_-$ are the corresponding eigenvectors, which have the form:

$$\mathbf{e}_+ = \begin{pmatrix} 1 \\ -(\alpha_1 - \lambda_+)/\alpha_2 \end{pmatrix} \quad \mathbf{e}_- = \begin{pmatrix} 1 \\ -(\alpha_1 - \lambda_-)/\alpha_2 \end{pmatrix} \tag{54}$$

and C_+ and C_- are unknown constants determined by the boundary conditions. The equilibrium temperatures, $T_{s,eqm}$ and $T_{j,eqm}$, of the sample and jacket are given by:

$$T_{s,eqm} = \frac{\alpha_3\beta_1 - \alpha_1\beta_3}{\alpha_2\beta_1 - \alpha_1\beta_2}, \quad T_{j,eqm} = \frac{\alpha_2\beta_3 - \alpha_3\beta_2}{\alpha_2\beta_1 - \alpha_1\beta_2} \tag{55}$$

Evaluating the eigenvalues using typical experimental data (Table 1) gives values for λ_+ and λ_- of $1.97 \times 10^{-4}\,s^{-1}$ and $8.81 \times 10^{-6}\,s^{-1}$ respectively. The time constants[(2)], τ_+ and τ_-, for each temperature distribution are obtained from the reciprocal of the eigenvalues, that is:

$$\tau_+ = \frac{1}{\lambda_+}, \quad \tau_- = \frac{1}{\lambda_-} \tag{56}$$

which gives values for τ_+ and τ_- of 5.08×10^3 s and 1.13×10^5 s respectively. The time constants τ_+ and τ_-, refer to the transient and asymtopic parts of each temperature distribution and, as one can see, the values for this system are several orders of magnitude greater than typical heating times (~ 15 s). The time constant τ_+ therefore represents the time for the sample to reach equilibrium with the graphite jacket, and the time for the sample and jacket to cool together to the environment temperature is given by τ_-.

---

(2) The time constant for a temperature distribution is the time required for the temperature to change by a factor of $1/e$.

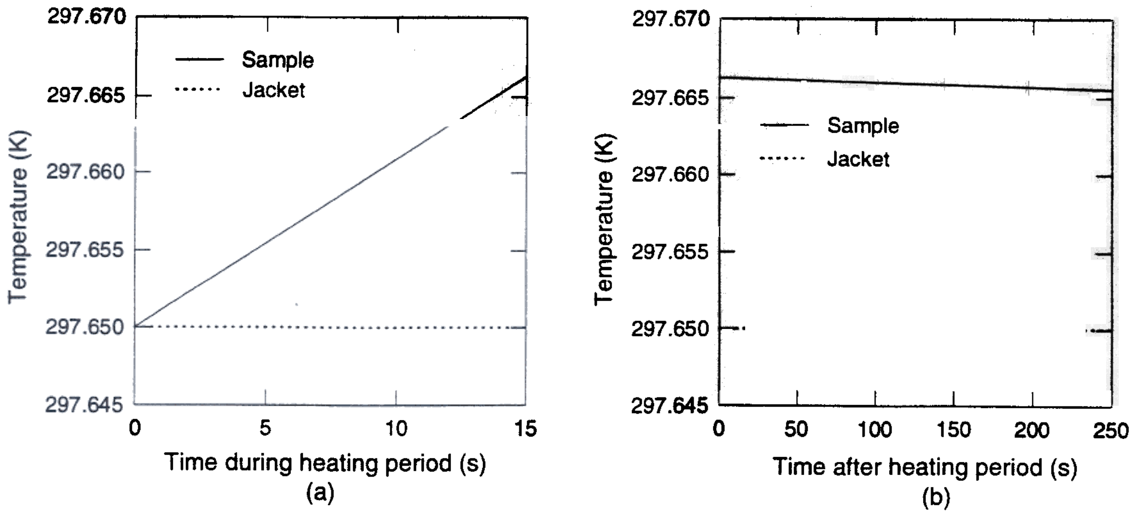

Figure 5 Variation of sample and jacket temperature with time: (a) during the heating period, and (b) after the heating period.

To obtain the actual variation of sample and jacket temperature during and after the heating period, boundary conditions need to applied to the general solution to determine values for the constants C_+ and C_-. If the sample and jacket are initially assumed to be at the same temperature as the environment (T_0), then C_+ and C_- have values of 6.245×10^{-2} K and -1.395 K during the heating period, and the temperature distributions of these components typically have the form shown in Figure 5(a). A sample heating time, t_{heat}, of 15.0 s has been used in this model with a power input, $\dot{E}_{in}$, of 39.0 mW (from Table 1). In this case, the equilibrium temperatures of the sample and jacket, $T_{s,eqm}$ and $T_{j,eqm}$, are 304.589 K and 298.983 K respectively, and the environment temperature T_0 is 297.650 K. From these distributions, one can see that the sample temperature increases more or less linearly during the heating period to 297.666 K (a rise of 16.323 mK) whereas, the temperature of the graphite jacket remains virtually constant (due to its much larger heat capacity).

The total energy lost by radiation from the sample surface, $E_{r,tot}$, during the heating period may be inferred from these temperature distributions using the following expression (for small temperature differences):

$$E_{r,tot} = 4\sigma T_0{}^3 F_s A_s \int_0^{t_{heat}} (T_s(t) - T_j(t))\, dt \qquad (57)$$

where F_s is given by equation (45), and $T_s(t)$ and $T_j(t)$ are the temperature distributions of the sample and jacket with time during heating. In this model, $E_{r,tot}$ has a value of 8.54×10^{-4} J. The total energy deposited into the sample is approximately 0.585 J ($\dot{E}_{in} \times t_{heat}$) and so approximately 0.15% of this energy is lost by radiation during the heating period.

The temperature distributions of the sample and jacket after the heating period are shown in Figure 5(b). These are obtained by assuming the initial temperatures of the sample and jacket are equal to their values at the end of the heating period, that is, 297.666 K and 297.650 K respectively. In this case, $\dot{E}_{in} = 0$ and the constants C_+ and C_- have values of -1.842×10^{-4} K and 1.845×10^{-4} K respectively. Both $T_{s,eqm}$ and $T_{j,eqm}$ are equal to the environment temperature T_0, as one would expect. As can be seen, the temperature of the sample gradually decreases with time after heating has been removed due to the radiative heat losses from the sample surface. The temperature of the jacket, however, has not changed from its equilibrium value.

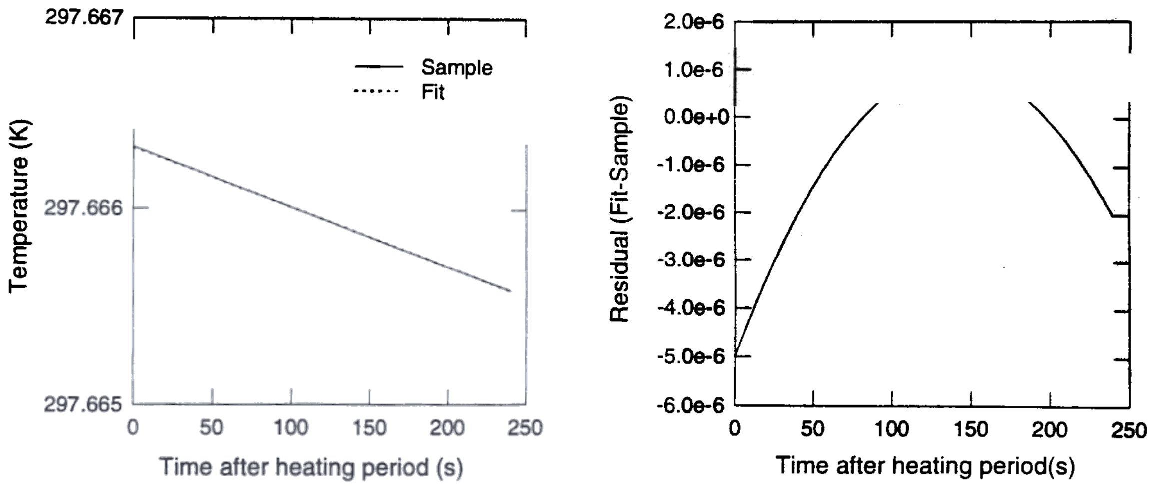

Figure 6 Linear least-squares fit to post-heating sample temperature data and corresponding residuals for the sample/jacket model.

7.2 EXTRAPOLATION OF DATA

Having determined the variation of sample temperature with time after the heating period, extrapolation techniques similar to those used in the experimental measurements will now be used to determine the 'measured' temperature rise of the sample $\Delta T_{s,m}$. In the measurements, the sample temperature is recorded at 0.4 s intervals before, during and after the heating period. The effect of heat losses are then eliminated by both linear and quadratic extrapolation of the pre-heating and post-heating temperature drifts to obtain the sample temperatures at the time during the heating period corresponding to the midpoint temperature rise. The 'measured' temperature rise of the sample is then the difference between these extrapolated temperatures.

The temperature rise of the sample in the model is obtained by first evaluating the post-heating sample temperature distribution at 0.4 s intervals over the range 40–240 s after the end of the heating period. This is the range typically used in the measurements for extrapolation of the post-heating data. Applying a linear least-squares fit to this data and extrapolating back to the midpoint heating time [3] (in this case, to $t = -t_{heat}/2$ s) gives a sample temperature of 297.666 K. Since there is no pre-heating temperature drift in the model (both sample and jacket are assumed to be initially at the same temperature as the environment, that is, 297.650 K), the 'measured' temperature rise of the sample $\Delta T_{s,m}$ is therefore 16.341 mK. With a quadratic least-squares fit, $\Delta T_{s,m}$ is 16.347 mK. Both the linear and quadratic fits to the post-heating sample temperature distribution and their residuals are shown in Figures 6 and 7. As can be seen, the residuals of quadratic fit are two orders of magnitude smaller than the linear fit over the whole range of times considered with both sets of residuals increasing only slightly near the beginning of the post-heating period. With no random noise in the temperature data,

[3]The midpoint heating time is used as the extrapolation point in the model whereas the midpoint temperature rise was used in the measurements. According to the model, the temperature of the sample has increased by 16.323 mK by the end of the heating period (from Section 7.1), and has reached it's midpoint temperature (8.162 mK) after 7.495 s. The difference between this time and the midpoint heating time (7.5 s) represents a change in $\Delta T_{s,m}$ of around 10^{-8} K, and so using midpoint heating time instead of midpoint temperature rise in the model makes no significant difference. One should note, however, that this analysis assumes a negligible time delay between the heat being applied to the sample and the corresponding temperature rise being detected by the sensing thermistor.

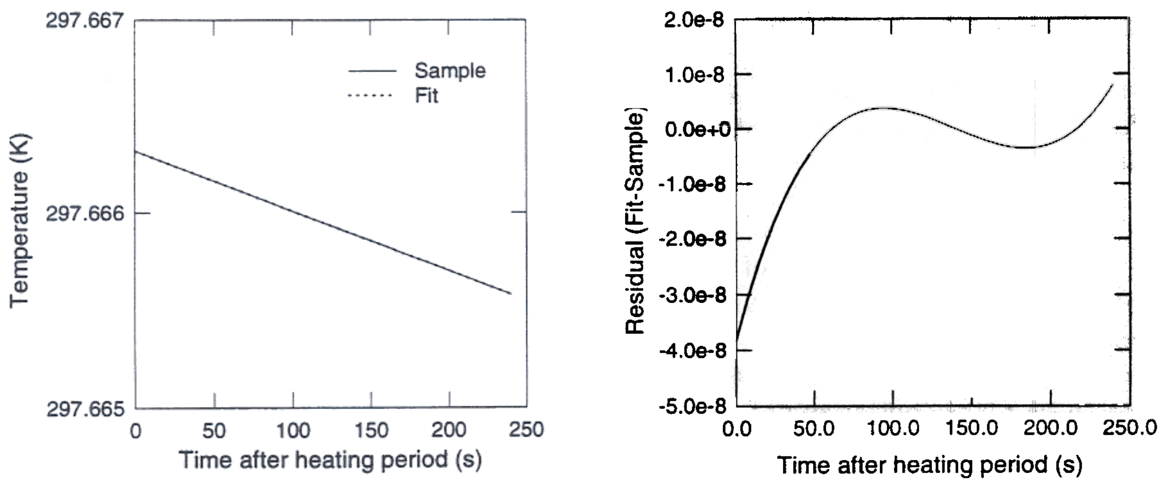

Figure 7 Quadratic least-squares fit to post-heating sample temperature data and corresponding residuals for the sample/jacket model.

one would therefore expect the quadratic fit to produce a slightly better estimate of sample temperature rise than the linear fit.

The rate at which the sample temperature decreases after heating (due to radiation losses) may be estimated from the slope of the linear fit. This has a value of $0.186\,\mathrm{mK\,min^{-1}}$ or $1.138 \times 10^{-2}\,\mathrm{mK\,min^{-1}}\ (\Delta T_{\mathrm{s,m}})^{-1}$ after normalising by the sample temperature rise. The corresponding experimental post-heating drift of the sample (after correcting for any pre-heating temperature drift) is typically $6.711 \times 10^{-3}\,\mathrm{mK\,min^{-1}}\ (\Delta T_{\mathrm{s,m}})^{-1}$ using the data given in Table 1. Thus the model used in this work and the actual measurement system agree to within about a factor of two.

The expected temperature rise of the sample, $\Delta T_{\mathrm{s,exp}}$, for a system with no heat losses is obtained using the following expression:

$$\Delta T_{\mathrm{s,exp}} = \left(\frac{\dot{E}_{\mathrm{in}}}{m_{\mathrm{s}} c_{\mathrm{s}}} \right) t_{\mathrm{heat}} \tag{58}$$

and for this model $\Delta T_{\mathrm{s,exp}}$ has a value of 16.346 mK. The difference between both 'measured' temperature rises and the expected rise are therefore very small (0.03% with the linear fit and less than 0.01% with the quadratic fit). One can therefore conclude that the corrections that need to be applied to the extrapolated temperature rise to obtain the actual temperature rise of the sample in the measurements are 1.0003 and 0.9999 for the linear and quadratic fits respectively. Since the model is believed to be a good representation of the sample/jacket measurement system (to within a factor of two), the uncertainty in each correction is estimated to be 0.01% (at 95% C.L.). Both these corrections are in fact much smaller than the estimated overall uncertainty in the experimental measurements (approximately 0.12% at 95% C.L.) and so can more or less be ignored.

8 CONCLUSIONS

The major source of heat loss in the measurements of specific heat capacity with the sample/jacket system is by radiation from the sample to the surrounding environment. The rate of heat transfer by this process is at least 100 times greater than the rate by any other mechanism of heat loss from the sample.

Analysis of the measurement system using a more realistic model (in which radiation is the only form of heat loss) indicates that corrections to extrapolated temperature rise are required to obtain the expected temperature rise of the sample. A correction of 1.0003 ± 0.0001 (95% C.L.) is required when a linear fit is used in the extrapolation and a correction of 0.9999 ± 0.0001 (95% C.L.) is required with a quadratic fit. In each case, the midpoint heating time was used as the extrapolation point instead of midpoint temperature rise (which was used in the experimental measurements). This makes no significant difference to the extrapolated temperatures. Assuming that the sample temperature at the position of the sensing thermistor is an accurate representation of the mean surface temperature of the sample (particularly during the heating period), these corrections account for all radiation losses in the measurement system. Examination of the post-heating temperature drifts also indicate that the sample/jacket model and the actual measurement system agree to within a factor of two.

Two other measurement systems considered during the course of the work have also been investigated (Appendix 1). Radiation losses from the sample surface are again the greatest source of heat loss in these systems but are larger in magnitude than in the sample/jacket system. The use of a second enclosure around the sample (with a large heat capacity) therefore tends to minimise the radiation losses from the sample.

Corrections to the extrapolated temperature rise of the sample are also required for each of these measurement systems. For the sample/mylar bag system, a correction of 1.0027 ± 0.0003 (95% C.L.) is required when a linear fit is used in the extrapolation and a correction of 1.0036 ± 0.0003 (95% C.L.) is required with a quadratic fit. For the sample without any form of enclosure, a correction of 1.0024 ± 0.0002 (95% C.L.) is required when a linear fit is used. With a quadratic fit, however, the correction required is negligible. In both cases, the model and measurement system agree to within 10%.

9 ACKNOWLEDGEMENTS

The authors would like to thank Alan DuSautoy for his helpful advice and criticism during the course of the this work.

10 REFERENCES

1 A J Williams, D T Burns, and M R McEwen. Measurement of the specific heat capacity of the electron beam graphite calorimeter. NPL Report RSA(EXT) 40, National Physical Laboratory, Teddington, Middlesex TW11 0LW, 1993.

2 R C L Bosworth. *Heat Transfer Phenomena*, chapter 5, pages 88–111. John Wiley & Sons, New York, 1952.

3 J S Laughlin and S Genna. Calorimetry. In F H Attix, W C Roesch, and E Tochilin, editors, *Radiation Dosimetry. Volume II: Instrumentation*, chapter 16, pages 389–441. Academic Press, New York, 1966.

4 W H McAdams. *Heat Transmission*, chapter 3, pages 45–86. McGraw-Hill, New York, second edition, 1942.

5 CRC. Emissivity of total radiation, ε_{tot}, for various materials. In R C Weast, M J Astle, and W H Beyer, editors, *CRC Handbook of Chemistry and Physics (64th edition)*, page E385. CRC Press, Florida, 1983-84.

Appendix 1 Other measurement systems

Two other experimental setups similar to the sample/jacket system were used during the course of the work to experimentally determine the specific heat capacity of the graphite sample. One setup used an aluminised mylar bag instead of the graphite jacket to completely enclose the sample inside the evacuated belljar. The bag was attached to the connecting thermistor leads and arranged such that there was no contact between the bag and sample surface. The other setup had no form of enclosure around the sample except the evacuated belljar. Analysis of the individual heat loss mechanisms in these systems using the same techniques as before (Sections 4 and 5) again indicated that radiation losses from the sample were by far the greatest source of heat loss in the experimental measurements. Each of these measurement systems will now be analysed using a more realistic model in this appendix (in a similar way to the sample/jacket system in Section 7) to determine whether any correction to the measured temperature rise is required.

A1.1 Sample enclosed in an aluminised mylar bag

The model that will be used for this setup is shown in Figure A1.1 and is very similar to that used in Section 7 for the sample/jacket system. It consists of a graphite sample, with an average surface temperature $T_s(t)$, enclosed in an aluminised mylar bag (of negligible thickness) at temperature $T_b(t)$, which is completely enclosed in an evacuated belljar held at a fixed environment temperature T_0. The inner surface of the belljar is again completely covered in aluminised mylar and is assumed to be in good thermal contact with this surface. The model also assumes that the sample has a high thermal conductivity and that the measured temperature of the sample represents the average surface temperature. With radiation assumed to be the only form of heat transfer in the system, one may write down the following two coupled first-order differential equations for the temperature distributions of the sample and bag (in the same way as in Section 7.1 for the sample/jacket system):

$$\begin{aligned}\frac{d}{dt}(T_b(t)) + \alpha_1 T_b(t) + \alpha_2 T_s(t) &= \alpha_3 \\ \frac{d}{dt}(T_s(t)) + \beta_1 T_b(t) + \beta_2 T_s(t) &= \beta_3\end{aligned}$$

where the parameters α_1–α_3 and β_1–β_3 are defined as follows:

$$\alpha_1 = \frac{4\sigma T_0{}^3(F_s A_s + F_b A_b)}{m_b c_b}, \quad \alpha_2 = -\frac{4\sigma T_0{}^3 F_s A_s}{m_b c_b}, \quad \alpha_3 = \frac{4\sigma T_0{}^4 F_b A_b}{m_b c_b}$$

$$\beta_1 = -\frac{4\sigma T_0{}^3 F_s A_s}{m_s c_s}, \quad \beta_2 = \frac{4\sigma T_0{}^3 F_s A_s}{m_s c_s}, \quad \beta_3 = \frac{\dot{E}_{in}}{m_s c_s}$$

The factors F_s and F_b for the sample and bag in these equations are given by:

$$\begin{aligned}F_s &= \frac{1}{(1/\varepsilon_s) + (A_s/A_b)[(1/\varepsilon_b) - 1]} \\ F_b &= \frac{1}{(1/\varepsilon_b) + (A_b/A_0)[(1/\varepsilon_0) - 1]}\end{aligned}$$

and

$\dot{E}_{in}$ is the rate at which the sample is heated (that is, the power input),

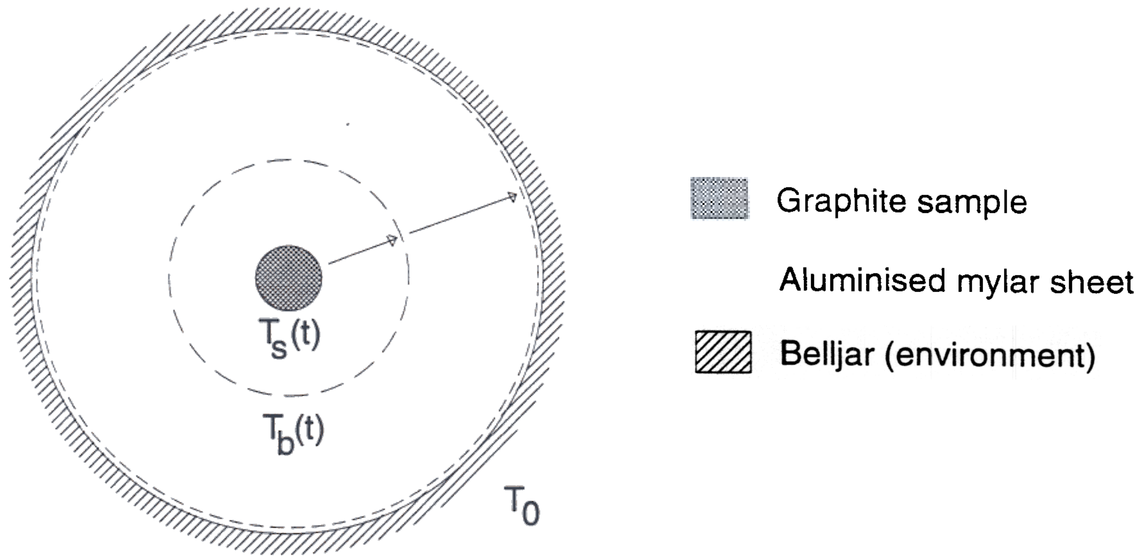

Figure A1.1 Model of the sample/mylar bag measurement system used to determine the variation of sample and bag temperature with time. Radiation is the only form of heat transfer in the system.

m_s, m_b are the masses of the sample and mylar bag,

c_s, c_b are the specific heat capacities of the sample and mylar bag,

A_s, A_b are the total surface areas of the sample and mylar bag,

A_0 is the total inner surface area of the belljar enclosure,

ε_s, ε_b are the emissivities of the sample and mylar bag surfaces, and,

ε_0 is the emissivity of the inner surface of the belljar.

The general solution of this system has a similar form to that for the sample/jacket system, that is:

$$\begin{pmatrix} T_b(t) \\ T_s(t) \end{pmatrix} = \begin{pmatrix} T_{b,eqm} \\ T_{s,eqm} \end{pmatrix} + C_+ \exp(-\lambda_+ t)\,\mathbf{e}_+ + C_- \exp(-\lambda_- t)\,\mathbf{e}_-$$

where λ_+ and λ_- are the eigenvalues of the system, $\mathbf{e}_+$ and $\mathbf{e}_-$ are the corresponding eigenvectors, and C_+ and C_- are unknown constants determined by the boundary conditions. The eigenvalues and eigenvectors for this system have the same form as for the sample/jacket system (equations (53) and (54)) but with the parameters α_1—α_3 and β_1—β_3 defined as in equations (61) and (62). The equilibrium temperatures, $T_{s,eqm}$ and $T_{b,eqm}$, of the sample and bag are given by:

$$T_{s,eqm} = \frac{\alpha_3\beta_1 - \alpha_1\beta_3}{\alpha_2\beta_1 - \alpha_1\beta_2}, \quad T_{b,eqm} = \frac{\alpha_2\beta_3 - \alpha_3\beta_2}{\alpha_2\beta_1 - \alpha_1\beta_2}$$

Evaluating the eigenvalues for the sample/bag system using typical experimental data gives values for λ_+ and λ_- of $3.20 \times 10^{-2}\,s^{-1}$ and $1.96 \times 10^{-4}\,s^{-1}$ respectively. The corresponding

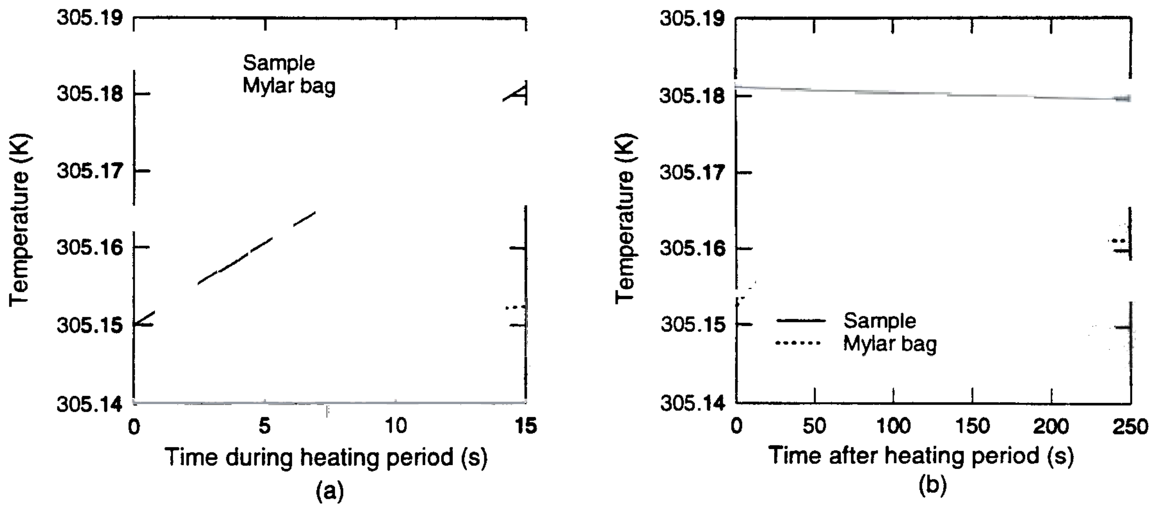

Figure A1.2 Variation of sample and mylar bag temperature with time: (a) during the heating period, and (b) after the heating period.

time constants, τ_+ and τ_-, therefore have values of 31.3 s and 5.10×10^3 s. τ_+ is more than two orders of magnitude smaller than the corresponding value for the sample/jacket system (5.1×10^3 s), and is now comparable to the typical heating times encountered in the experimental measurements. One would therefore expect the temperature of the mylar bag to increase significantly towards its equilibrium value during the heating period. Similarly, τ_- is also significantly smaller than the corresponding asymtopic value for the sample/jacket system. The time constant τ_+ therefore represents the time for the mylar bag to reach equilibrium with the sample in this system, and τ_- is the time for the sample and bag to cool together to the environment temperature.

If the sample and bag are initially assumed to be at the same temperature as the environment, then the temperature distributions of the sample and bag during the heating period typically have the form shown in Figure A1.2(a). Here, $\dot{E}_{in}$ = 78.0 mW and t_{heat} = 15 s, and the enviroment temperature T_0 is fixed at 305.15 K. The parameters C_+ and C_- have values of 2.465×10^{-2} K and −4.023 K respectively, and, $T_{s,eqm}$ and $T_{b,eqm}$ are 315.750 K and 309.149 K. The sample temperature in the model again increases more or less linearly during the heating period to approximately 305.181 K. The temperature of the mylar bag enclosure also increases slightly particularly towards the end of the heating period (unlike the jacket enclosure in the sample/jacket system where the heat capacity of the enclosure is much larger). The total energy lost from the sample by radiation during the heating period, $E_{r,tot}$, is typically 2.62×10^{-3} J (using equation (57) with $T_b(t)$ instead of $T_j(t)$). The energy input is 1.170 J ($\dot{E}_{in} \times t_{heat}$) and so approximately 0.22% of the energy deposited in the sample is radiated in this system.

The temperature distributions of the sample and bag after the heating period in this model are shown in Figure A1.2(b). In this case, $\dot{E}_{in} = 0$, $T_{s,eqm} = T_{b,eqm} = T_0$, and C_+ and C_- have values of -9.397×10^{-3} K and 1.182×10^{-2} K respectively. As soon as heating has been removed, the sample temperature gradually decreases towards the environment temperature, whereas the bag temperature continues to increase for approximately 150 s after the end of the heating period. This behaviour is primarily due to the bag enclosure having such a small heat capacity. Ideally, the heat capacity of the enclosure should be several orders of magnitude larger than that of the sample (as in the sample/jacket system) so that any change in the behaviour of the sample has no significant influence on the surrounding enclosure.

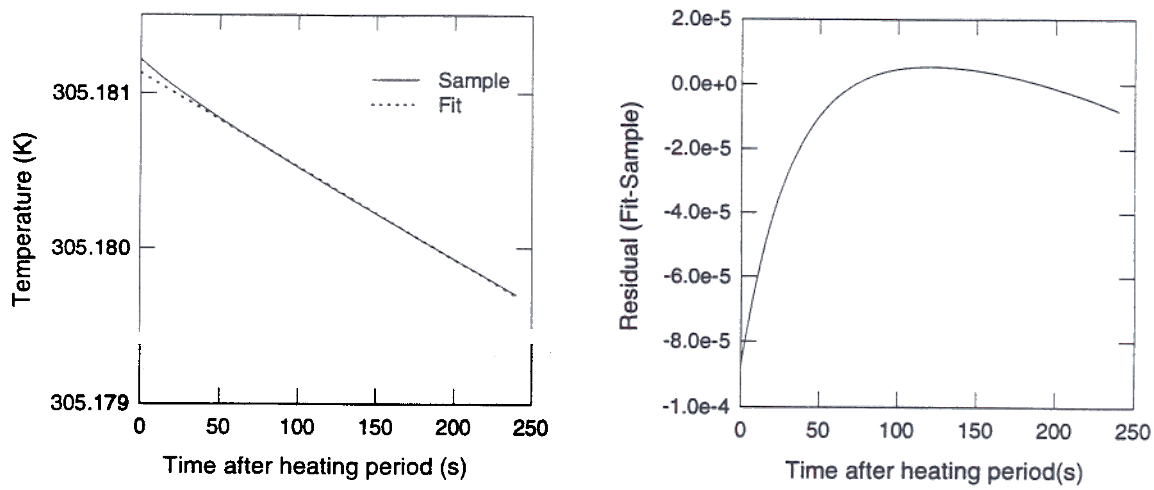

Figure A1.3 Linear least-squares fit to post-heating sample temperature data and corresponding residuals for the sample/mylar bag model.

The 'measured' temperature rise of the sample, $\Delta T_{s,m}$, in the model may be estimated using extrapolation techniques similar to those used in the experimental measurements. The methods that were used for this system are the same as those used for the sample/jacket system and are discussed in Section 7.2. Applying a linear least-squares fit to the post-heating sample temperature data in the model and extrapolating back to the midpoint heating time gives a sample temperature of 305.181 K. With no pre-heating temperature drift in this model (both sample and bag initially assumed to be at the environment temperature T_0), the 'measured' temperature rise of the sample $\Delta T_{s,m}$ is 31.178 mK. This temperature rise is twice the rise observed in the model of the sample/jacket system because the power input here has been doubled. The value obtained for $\Delta T_{s,m}$ with a quadratic fit is 31.208 mK. The linear and quadratic fits to the post-heating sample data and their residuals are shown in Figures A1.3 and A1.4, and, as can be seen, the residuals in both cases are again very small over the fitted range of values but they are substantially larger near the beginning of the post-heating period (and at least one order of magnitude greater than in the sample/jacket model). This would indicate that a larger correction to the extrapolated temperature rise is required in this system.

The post-heating temperature drift of the sample in the model may be estimated from the slope of the linear fit. This has a value of 0.361 mK min^{-1} or 1.158×10^{-2} mK min^{-1} $(\Delta T_{s,m})^{-1}$ and compares with a corrected experimental post-heating drift of 0.329 mK min^{-1} or 1.048×10^{-2} mK min^{-1} $(\Delta T_{s,m})^{-1}$. Again, there is reasonable agreement between the model and the actual measurement system, this time to within 10%.

The expected temperature rise of the sample, $\Delta T_{s,exp}$, in the model (with no heat losses) is 31.291 mK (using equation (58)). The extrapolated temperature rise using a linear fit is thus approximately 0.36% less than the expected rise, and using a quadratic fit, approximately 0.27% less than the expected rise. These discrepancies are much greater than the estimated overall uncertainty in the experimental measurements (0.12% at 95% C.L.) and so a correction must be applied to the measured temperature rise of the sample to obtain the expected value. The correction factor with a linear fit is therefore 1.0036 and with a quadratic fit is 1.0027. Since the model and measurement system agree to within 10%, the uncertainty in each factor is perhaps 0.03% (at 95% C.L.).

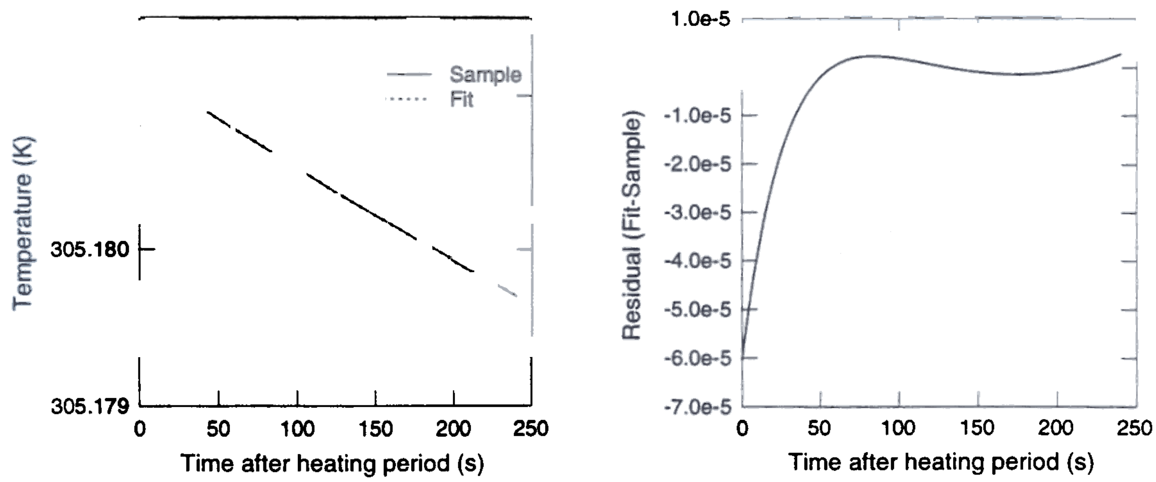

Figure A1.4 Quadratic least-squares fit to post-heating sample temperature data and corresponding residuals for the sample/mylar bag model.

A1.2 Sample without an enclosure

The model shown in Figure A1.5 will be used here to investigate the behaviour of this system. The analysis will be much simpler than before since one only needs to consider the temperature distribution of the sample. The model consists of a graphite sample, with an average surface temperature $T_s(t)$ and negligible relaxation time, completely enclosed in an evacuated belljar held at a constant temperature T_0. The inner surface of the belljar is lined with aluminised mylar assumed to be in good thermal contact and radiation is assumed to be the only form of heat transfer. The two differential equations governing the rate of heat flow in the model are as follows:

$$\dot{E}_{r,s0} \equiv \left.\frac{dE}{dt}\right|_{r,s0} = A_s \sigma F_s([T_s(t)]^4 - T_0^4)$$

$$\dot{E}_{in} - \dot{E}_{r,s0} = m_s c_s \frac{d}{dt}(T_s(t))$$

where the factor F_s for the sample is given by:

$$F_s = \frac{1}{(1/\varepsilon_s) + (A_s/A_0)[(1/\varepsilon_0) - 1]} \tag{69}$$

and

$\dot{E}_{r,s0}$ is the net rate of heat flow by radiation between the sample and the belljar,

$\dot{E}_{in}$ is the rate at which the sample is heated (that is, the power input),

m_s is the mass of the sample,

c_s is the specific heat capacity of the sample,

A_s is the total surface area of the sample,

A_0 is the total inner surface area of the belljar enclosure,

ε_s is the emissivity of the sample surface, and,

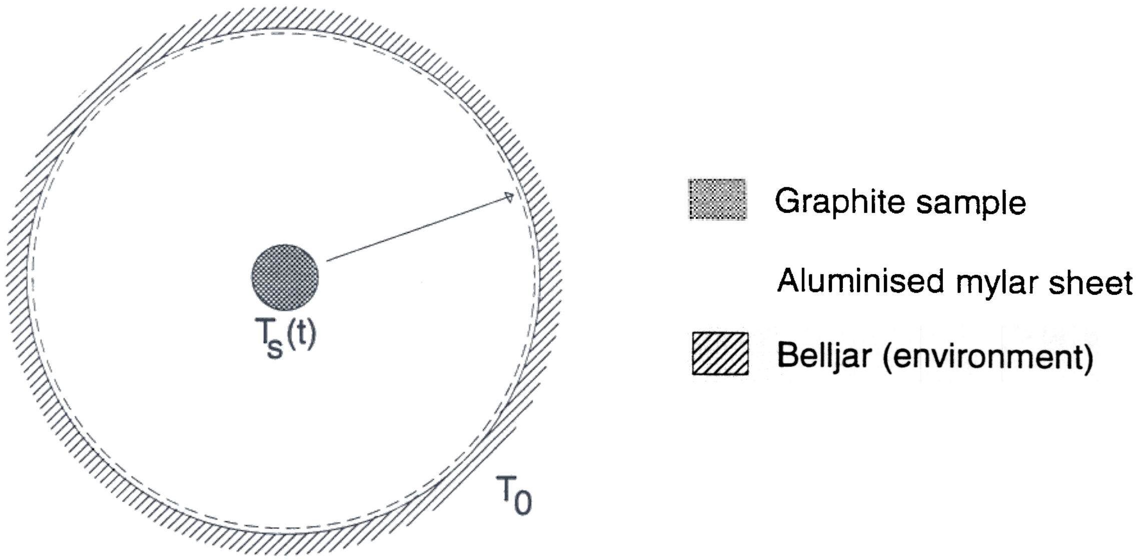

Figure A1.5 Model of the measurement system without any form of enclosure around the sample (except the belljar). Radiation is the only form of heat transfer in the system.

ε_0 is the emissivity of the inner surface of the belljar.

Combining these two equations and rearranging gives the following first-order linear differential equation (when $T_s \approx T_0$):

$$\frac{d}{dt}(T_s(t)) + \alpha_1 T_s(t) = \alpha_2$$

where the parameters α_1 and α_2 are defined as:

$$\alpha_1 = \frac{4\sigma T_0{}^3 F_s A_s}{m_s c_s}, \quad \alpha_2 = \frac{\dot{E}_{in} + 4\sigma T_0{}^4 F_s A_s}{m_s c_s}$$

The general solution to this equation for the temperature distribution of the sample has the form:

$$T_s(t) = T_{s,eqm} + C\exp(-\lambda t)$$

where the equilibrium temperature of the sample $T_{s,eqm}$ and the decay constant for the distribution λ are given by:

$$T_{s,eqm} = \frac{\alpha_2}{\alpha_1}, \quad \lambda = \alpha_1$$

Evaluating λ using typical values encountered in the experimental measurements gives a value of $5.31 \times 10^{-4}\,s^{-1}$ and thus the time constant τ of the sample is 1.88×10^3 s. This is two orders of magnitude greater than typical heating times and thus one would expect the sample temperature to increase only slightly towards its equilibrium value during the heating period.

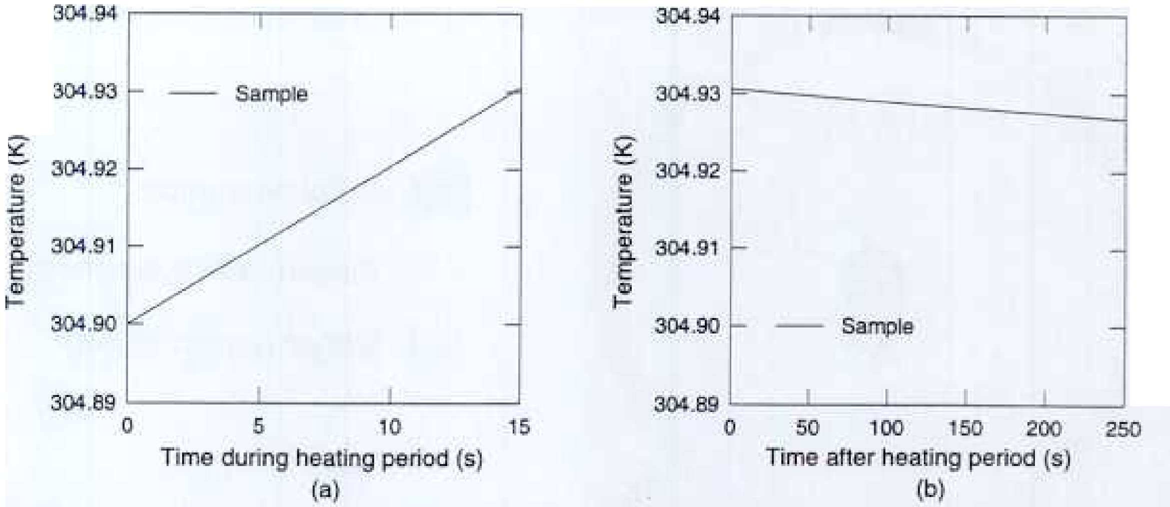

Figure A1.6 Variation of sample temperature with time: (a) during the heating period, and (b) after the heating period.

It is also much smaller than the asymtopic time constants (τ_{-}) in the sample/jacket and sample/bag systems. The rate at which the system cools towards the environment temperature after the heating period is therefore expected to be much greater for this system.

The temperature distribution of the sample during the heating period typically has the form shown in Figure A1.6(a) (assuming that the sample and environment are initially at the same temperature). With $\dot{E}_{in}$ = 76.5 mW, t_{heat} = 15 s and T_0 = 304.9 K, the unknown constant C has a value of −3.856 K and the equilibrium temperature of the sample $T_{s,eqm}$ is 308.756 K. As can be seen from this distribution, the temperature of the sample again rises almost linearly during the heating period. The total energy lost from the sample by radiation during this period is estimated to be 4.56×10^{-3} J (using equation (57)). Approximately 0.40% of the input energy (1.148 J) is therefore radiated which is almost twice the energy radiated in the sample/bag system (~ 0.22%) is radiated). This suggests that the presence of a second enclosure around the sample tends to significantly reduce radiative heat losses.

After the heating period, the temperature distribution of the sample has the form shown in Figure A1.2(b). Here $\dot{E}_{in} = 0$, $T_{s,eqm} = T_0$ and the constant C has a value of 3.060×10^{-2} K. The sample temperature gradually decreases with time towards the environment temperature due to radiative heat losses from the sample surface.

The 'measured' temperature rise of the sample, $\Delta T_{s,m}$, in the model is obtained as before using extrapolation techniques similar to those used in the experiments (Section 7.2). With a linear least-squares fit applied to the post-heating temperature data, the extrapolated temperature at the midpoint heating time is 304.931 K. The 'measured' temperature rise $\Delta T_{s,m}$ is therefore 30.643 mK (since there is no pre-heating drift in the model and the sample is initially assumed to be at the same temperature as the environment). With a quadratic fit, $\Delta T_{s,m}$ is 30.716 mK. The linear and quadratic fits to the post-heating sample data and their residuals are shown in Figures A1.7 and A1.8. As can be seen, the residuals associated with the quadratic fit are at least one order of magnitude smaller than those associated with the linear fit particularly at the beginning of the post-heating period. The quadratic fit should therefore produce a much better estimate of the expected temperature rise of the sample.

The post-heating temperature drift of the sample in this model is obtained from the slope of the linear fit and has a value of 0.905 mK min^{-1} or 2.953×10^{-2} mK min^{-1} $(\Delta T_{s,m})^{-1}$. The mea-

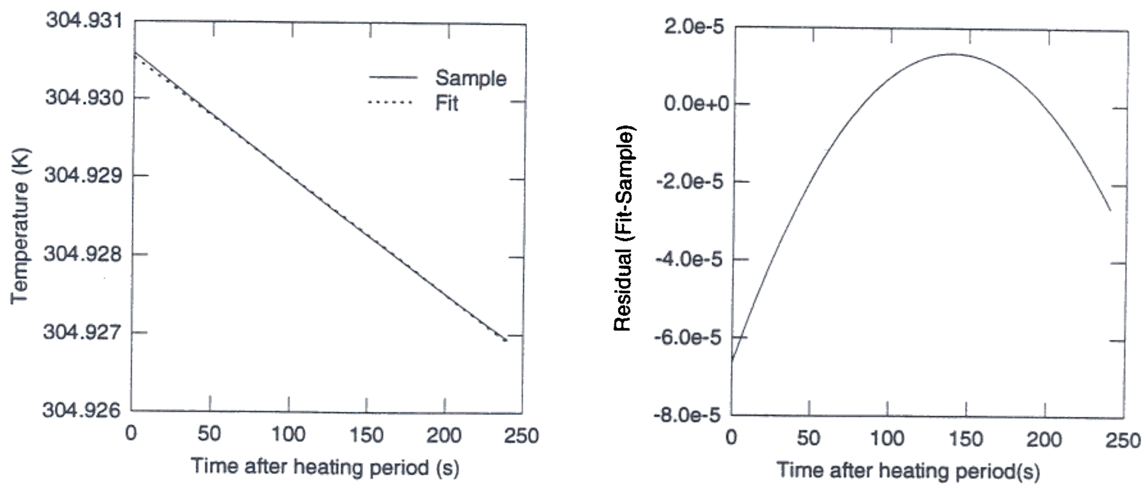

Figure A1.7 Linear least-squares fit to post-heating sample temperature data and corresponding residuals for the sample without enclosure model.

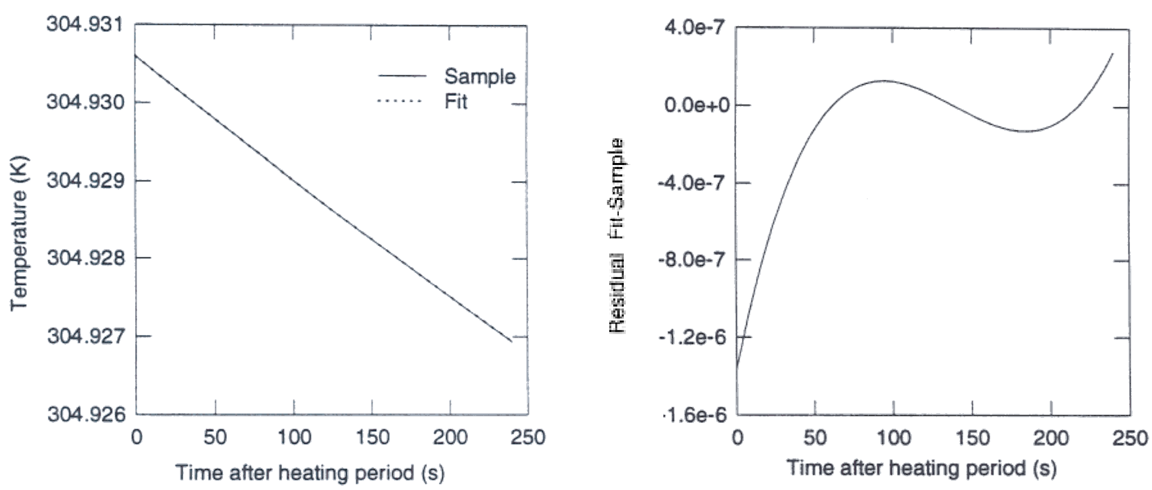

Figure A1.8 Quadratic least-squares fit to post-heating sample temperature data and corresponding residuals for the sample without enclosure model.

sured post-heating drift is $0.843\,\mathrm{mK\,min^{-1}}$ or $2.749\,\mathrm{mK\,min^{-1}}$ $(\Delta T_{s,m})^{-1}$ (after correction for pre-heating drift) and is within 10% of the model value. These drift values are 2–3 times greater than the post-heating temperature drifts observed in the sample/jacket and sample/bag measurement systems thus confirming that heat losses tend to be reduced when the sample has some form of enclosure.

The expected temperature rise of the sample, $\Delta T_{s,exp}$, (with no heat losses) is $30.718\,\mathrm{mK}$ (using equation (58)). The 'measured' temperature rise in this model with a linear fit is therefore 0.24% less than the expected rise. This is larger than the estimated uncertainty in the experimental measurements (0.12% at 95% C.L.) and so a correction of 1.0024 needs to be applied to the measured temperature rise of the sample in this case. With a quadratic fit, however, the discrepancy between the extrapolated temperature rise in the model and the expected rise is $< 0.01\%$. The correction required in this case is negligible (< 1.0001) and can be ignored since this difference is much smaller than the experimental uncertainty. The agreement between the model and the measurement system is better than 10% and so the uncertainty in each correction is perhaps 0.02% (at 95% C.L.).